Biogeosciences

A ^{13}C labelling study on carbon fluxes in Arctic plankton communities under elevated CO$_2$ levels

A. de Kluijver[1], K. Soetaert[1], J. Czerny[2], K. G. Schulz[2], T. Boxhammer[2], U. Riebesell[2], and J. J. Middelburg[1,3]

[1]Department of Ecosystems Studies, Royal Netherlands Institute for Sea Research (NIOZ), Yerseke, the Netherlands
[2]Helmholtz Centre for Ocean Research Kiel (GEOMAR), Kiel, Germany
[3]Faculty of Geosciences, Utrecht University, Utrecht, the Netherlands

Correspondence to: A. de Kluijver (anna.dekluijver@deltares.nl)

Abstract. The effect of CO$_2$ on carbon fluxes (production, consumption, and export) in Arctic plankton communities was investigated during the 2010 EPOCA (European project on Ocean Acidification) mesocosm study off Ny Ålesund, Svalbard. ^{13}C labelled bicarbonate was added to nine mesocosms with a range in pCO$_2$ (185 to 1420 µatm) to follow the transfer of carbon from dissolved inorganic carbon (DIC) into phytoplankton, bacterial and zooplankton consumers, and export. A nutrient–phytoplankton–zooplankton–detritus model amended with ^{13}C dynamics was constructed and fitted to the data to quantify uptake rates and carbon fluxes in the plankton community. The plankton community structure was characteristic for a post-bloom situation and retention food web and showed high bacterial production ($\sim$ 31 % of primary production), high abundance of mixotrophic phytoplankton, low mesozooplankton grazing ($\sim$ 6 % of primary production) and low export ($\sim$ 7 % of primary production). Zooplankton grazing and export of detritus were sensitive to CO$_2$: grazing decreased and export increased with increasing pCO$_2$. Nutrient addition halfway through the experiment increased the export, but not the production rates. Although mixotrophs showed initially higher production rates with increasing CO$_2$, the overall production of POC (particulate organic carbon) after nutrient addition decreased with increasing CO$_2$. Interestingly, and contrary to the low nutrient situation, much more material settled down in the sediment traps at low CO$_2$. The observed CO$_2$ related effects potentially alter future organic carbon flows and export, with possible consequences for the efficiency of the biological pump.

1 Introduction

About 30 % of anthropogenic CO$_2$ has accumulated in the oceans, causing the modification of the ocean's chemistry. The most important impacts of anthropogenic CO$_2$ on marine carbonate chemistry are higher concentrations of CO$_2$ and a concurrent drop in pH, collectively referred to as ocean acidification. The CO$_2$ uptake capacity of the oceans is influenced by the plankton organisms that live in the surface waters. The flux of CO$_2$ from atmosphere to oceans is largely controlled by three biological processes: primary production, community respiration, and export (biological pump). Primary production and subsequent sinking of organic matter (OM) to depth increases the ocean's uptake capacity for CO$_2$. Community respiration in the upper ocean, dominated by heterotrophic bacteria, converts organic carbon back into CO$_2$ and thus decreases the ocean's CO$_2$ uptake capacity (Rivkin and Legendre, 2001). Understanding the effects of increasing CO$_2$ levels on these three processes is central to predicting the ocean's response to rising atmospheric pCO$_2$. Particularly, production and export showed to be potentially sensitive to changes in CO$_2$ (Riebesell et al., 2009).

The high-latitude oceans are especially vulnerable for anthropogenic CO$_2$ disturbances because of lower temperatures. The solubility of CO$_2$ increases with decreasing temperatures, so that polar oceans contain naturally high CO$_2$ and low carbonate ion concentrations. With a lower buffer capacity, pH changes are considerably larger in the polar regions than at lower latitudes for future climate scenarios (Steinacher et al., 2009). Our knowledge about the potential effects of ocean acidification on plankton

communities in polar regions is limited, but plankton community studies have been done in mid-latitude regions. In a mesocosm experiment in a Norwegian Fjord (Bergen, 2005), an increased inorganic carbon consumption relative to nutrient (N, P) uptake was observed at higher CO_2 levels in natural plankton communities (Riebesell et al., 2007; Bellerby et al., 2008). The enhanced uptake was not reflected in increased organic matter production (Schulz et al., 2008; de Kluijver et al., 2010) nor in increased bacterial activity (Algaier et al., 2008; de Kluijver et al., 2010) so enhanced export was the suggested sink for the extra carbon consumed at elevated pCO$_2$ (Riebesell et al., 2007). A proposed mechanism is that CO_2 induced carbon overconsumption is exuded by phytoplankton as dissolved organic matter (DOM), which aggregates with other particles and increases export (Engel et al., 2004a). In another mesocosm experiment (Bergen, 2001) no CO_2 effects on primary production (DeLille et al., 2005) were recorded, but a stimulating effect of CO_2 on bacterial activity was observed (Engel et al., 2004b; Grossart et al., 2006). In the mesocosm studies mentioned above, nutrients were added to stimulate phytoplankton production at the start of the experiments, so CO_2 effects on a eutrophic, blooming community were observed. However, throughout most of the year, plankton communities exist under low nutrient conditions dominated by regenerated production, rather than new production (Legendre and Rassoulzadegan, 1995).

This mesocosm study is the first to investigate the effects of elevated CO_2 on high-latitude plankton communities and on plankton communities in a post-bloom, nutrient regenerating state. In summer 2010, nine mesocosms were set up in Kongsfjorden, Svalbard, with a range of CO_2 levels and monitored for changes in plankton community functioning. To study the uptake of carbon by phytoplankton (primary production) and subsequent transfer to bacteria and zooplankton (community respiration) and settling material (export), ^{13}C-DIC (dissolved inorganic carbon) was added as a tracer.

The ^{13}C labelling dynamics of phytoplankton and bacteria were determined by compound-specific isotope analyses of polar lipid fatty acid (PLFA) biomarkers. Groups of phytoplankton and bacteria produce characteristic fatty acids, so the abundance and enrichment of these fatty acids can be used as proxies for biomass and label incorporation in these groups, respectively (Boschker and Middelburg, 2002). Because PLFA are membrane fatty acids, which degrade rapidly after cell death, they are more suitable as a proxy for total biomass than, for example, storage lipids (Boschker and Middelburg, 2002). The technique has been successfully applied in the previous CO_2 enrichment mesocosm experiment (Bergen, 2005) to study the interactions between phytoplankton and bacteria (de Kluijver et al., 2010). In addition to the previous mesocosm experiment (Bergen, 2005), ^{13}C POC and zooplankton analyses as well as quantitative sediment trap samples were included in this mesocosm study. A nutrient–phytoplankton–zooplankton–detritus model was constructed to quantify uptake and loss parameters and carbon flows in the mesocosms. The obtained parameters and fluxes were tested for CO_2 sensitivity.

2   Materials and methods

2.1   Experimental setup and sampling

The mesocosm experiment was carried out in Kongsfjorden, Svalbard (78°56,2' N, 11°53,6' E), in June–July 2010 as part of the 2010 EPOCA (European project on Ocean Acidification) Arctic campaign. The experimental setup and mesocosm characteristics are described in detail in Riebesell et al., 2012; Czerny et al., 2012a. Briefly, 9 mesocosms of $\sim 50\,\text{m}^3$ were deployed in the Kongsfjorden, about a mile off Ny Ålesund, on 28 May 2010. While lowering to $\sim 15\,\text{m}$ depth, the bags filled with nutrient-poor, post-bloom fjord water. A 3 mm mesh size net was used to exclude large organisms. The bags were closed on 31 May 2010, defined as time t_{-7} and time steps (t) continued per day. The CO_2 manipulation was done in steps over 5 days, from t_{-1} to t_4, by adding calculated amounts of CO_2 enriched seawater to each mesocosm. The main additions were done from t_{-1} to t_2 and a final adjustment was done on t_4. A range of initial pCO$_2$ levels of ~ 185–$1420\,\mu$atm was achieved (exact CO_2 levels are provided in Bellerby et al., 2012). Due to gas exchange and photoautotrophic uptake, pCO$_2$ levels declined in the mesocosms, especially in the high CO_2 treatments, to a final pCO$_2$ range from ~ 160–$855\,\mu$atm at the end of the experiment. ^{13}C-bicarbonate (10 g per mesocosm), corresponding to ~ 0.1 % of DIC, was added to the mesocosms together with the first CO_2 addition (t_{-1}), increasing the δ^{13}C signature of DIC by ~ 100 ‰ to stimulate phytoplankton production. The total added concentrations were 5 μM nitrate, 0.32 μM phosphate, and 2.5 μM silicate. The experiment was terminated at t_{30}. The experimental period was divided into three phases based on the applied perturbations and Chl a dynamics. Phase 1 was before nutrient addition (t_{4-13}). Phase 2 was after nutrient addition until the 2nd Chl a minimum (t_{14-21}) and phase 3 was from the 2nd Chl a minimum until the end of the experiment (t_{22-29}) (Schulz et al., 2012). In this manuscript we only consider two phases, phase 1 before nutrient addition (t_{0-12}) and phase 2 after nutrient addition (t_{14-29}).

Depth-integrated samples (0–12 m) were taken each morning (9–11 h), with an integrating water sampler (IWS; Hydrobios, Kiel, Germany), for most parameters, including nutrients, chlorophyll, particulate organic carbon, phosphate, and nitrogen (POC, POP, PON), dissolved organic carbon, phosphate, and nitrogen (DOC, DOP, DON), dissolved inorganic carbon (DIC), and ^{13}C content of carbon pools (DIC, DOC, POC, biomarkers). Daily samples for ^{13}C-DIC and ^{13}C-DOC were taken directly from the IWS and stored in dark, gastight glass bottles. The sediment traps were emptied every other day before daily routine sampling and processed as

described in (Czerny et al., 2012a). Zooplankton samples were taken weekly, in the afternoon, by vertical 55 µm mesh size Apstein net hauls over the upper 12 m.

Daily ^{13}C-polar lipid fatty acid (PLFA) samples were collected on pre-combusted 47 mm GF/F filters by filtering ~ 3–4 L and filters were stored at $-80\,^\circ$C. Daily ^{13}C-POC samples were collected on pre-weighted and pre-combusted 25 mm GF/F filters by filtering ~ 0.5 L, filters were subsequently stored at $-20\,^\circ$C and freeze-dried afterwards. From the gas-tight water samples, headspace vials (20 mL) were filled using an overflow method and sealed with gas-tight caps for DIC isotope analyses. Mercury chloride was added for preservation and the samples were stored upside down at room temperature. Samples for dissolved organic carbon (DOC) were GF/F filtered and stored frozen (-20°) in clean (HCl and mQ rinsed) vials until further analyses. Zooplankton were transferred to filtered seawater and kept there for a minimum of 3 h to empty their guts. On average, 7 (range 1–30) individuals of *Calanus* sp. and 30 (range 16–35) individuals of *Cirripedia* larvae were handpicked and transferred to pre-combusted tin cups (200 $^\circ$C, 12 h), which were subsequently freeze-dried. Zooplankton samples were analyzed for organic ^{13}C content. Subsamples of freeze-dried and homogenized sediment trap material were analyzed for total organic ^{13}C. Sediment trap material of the last 8 days (t_{22-30}) was additionally analyzed for ^{13}C-PLFA to characterize the nature of settling material.

2.2 Laboratory analyses

POC, sediment trap material and zooplankton samples were analyzed for organic carbon content and isotope ratios on a Thermo Electron Flash EA 1112 analyser (EA) coupled to a Delta V isotope ratio mass spectrometer (IRMS). For DIC isotope analyses, a helium headspace was added to the headspace vials and samples were acidified with H_3PO_4 solution. After equilibration, the CO_2 concentration and isotope ratio in the headspace was measured on EA-IRMS. PLFA were extracted using a modified Bligh and Dyer method (Bligh and Dyer, 1959; Middelburg et al., 2000). The lipids were fractionated in different polarity classes by column separation on a heat activated silicic acid column and subsequent elution with chloroform, acetone and methanol. The methanol fractions, containing most of the polar lipid fatty acids were collected and derivatized to fatty acid methyl esters (FAME). The standards 12:0 and 19:0 were used as internal standards. Concentrations and δ^{13}C of individual PLFA were measured using gas chromatography-combustion isotope ratio mass spectrometry (GC-C-IRMS) (Middelburg et al., 2000; de Kluijver et al., 2010).

2.3 Data analyses

Carbon stable isotope ratios are expressed in the delta notation relative to Vienna Pee Dee Belemnite (VPDB) standard (δ^{13}C). Relative (^{13}C) incorporation in carbon samples is presented as $\Delta\delta^{13}$C ^{13}C$_{sample} - \delta^{13}$C$_{background}$. Absolute label incorporation was calculated as ^{13}C concentration $= \Delta^{13}$F $\times$ concentration (µmol C L^{-1}), with Δ^{13}F being ^{13}F$_{sample} - ^{13}$F$_{background}$, and ^{13}F being the ^{13}C fraction (^{13}C/(^{12}C $+ ^{13}$C)) derived from the delta notation. δ^{13}C$_{background}$ and ^{13}F$_{background}$ are the natural abundance isotope ratios, which were sampled before label addition. To compare ^{13}C concentrations of organic carbon pools between mesocosms, the data were corrected for small differences in initial ^{13}C DIC concentrations using a correction factor. The correction factor was calculated from deviations of ^{13}C-DIC from the average ^{13}C-DIC on day 3 (after main CO_2 additions) and ranged from 0.89 to 1.08. This correction is used for clarity of presentation and was not used for model calculations. ^{13}C-DIC results were corrected for gas exchange according to Czerny et al. (2012b). The δ^{13}C of CO_2 [aq] was calculated according to Zhang et al. (1995) and the δ^{13}C of atmospheric CO_2 was assumed as -8 ‰.

$\Delta\delta^{13}$C PLFA of phytoplankton showed 2 responses of ^{13}C incorporation: rapid label incorporation and more gradual label incorporation. Phytoplankton were therefore separated into 2 groups (phytoplankton and mixotrophs) (Fig. 1a). The rapidly incorporating PLFA were 18:3ω3, 18:4ω3, 18:5ω3(12–15), 18:5ω3(12–16), and 16:4ω3 and their weighted average (Δ)δ^{13}C was used to determine (Δ)δ^{13}C of autotrophic phytoplankton, hereafter phytoplankton. The PLFA with delayed incorporation were 20:5ω3, 22:6ω3, and 16:4ω1 and their weighted average (Δ)δ^{13}C was used to determine (Δ)δ^{13}C of mixotrophic (phytoplankton), hereafter mixotrophs. PLFA present in phytoplankton is characteristic for green algae, prymnesiophytes (haptophytes), cryptophytes, and autotrophic dinoflagellates. PLFA of mixotrophs is characteristic for diatoms and (heterotrophic) dinoflagellates (Dijkman et al., 2009). It was possible to distinguish between autotrophic dinoflagellates and total dinoflagellates, because 18:5ω3 is considered a chloroplast fatty acid, while 22:6ω3 is a cell membrane lipid (Adolf et al., 2007). The branched fatty acids i15:0, ai15:0, and i17:0 were used to characterize heterotrophic bacteria. These fatty acids occur primarily in gram-positive bacteria (Kaneda, 1991), although they are found in gram-negative bacteria as well (Zelles et al. 1999). The last step involved conversion from PLFA biomass to total organic carbon (OC) concentration for each group. The conversion factor for phytoplankton was calculated as 0.06 (sum PLFA:OC) and 0.05 (sum PLFA:OC) for mixotrophs, based on phytoplankton culture and literature values (Dijkman et al., 2006). The conversion factor for bacterial carbon was 0.01 (sum PLFA/OC) (van den Meersche et al., 2004). The conversion factors were kept constant during the experiment.

Group specific daily growth rates (μ,d^{-1}) were calculated according to Dijkman et al. (2009) as

$$\mu\left(\text{days}^{-1}\right) = \ln\left(\frac{^{13}C_{\text{concentration}_{t\to\Delta t}}}{^{13}C_{\text{concentration}_t}}/\text{cf}\right) \qquad (1)$$

$$\text{cf} = \text{mean}\left(1 - \frac{\Delta\delta^{13}C_{\text{organism}_t}}{\Delta\delta^{13}C_{\text{DIC}_t}}\right)_{t\to t+\Delta t}. \qquad (2)$$

The correction factor (cf) is necessary to correct for label saturation and represents the difference between organism (phytoplankton, mixotrophs and bacteria) and DIC labelling ($\Delta\delta^{13}C$) relative to the $\Delta\delta^{13}C$ of DIC averaged over the considered growth period for each mesocosm. Production rates were calculated as

$$P\left(\mu\text{mol C L}^{-1}\text{days}^{-1}\right) = \frac{\Delta^{13}F_{\text{producer}}}{\Delta^{13}F_{\text{DIC}}} \times \frac{C_{\text{producer}}}{t} \qquad (3)$$

2.4 Model

A nutrient–phytoplankton–zooplankton–detritus (NPZD) model, amended with isotope values, was constructed to quantify carbon fluxes within the plankton food web. The model is based on those of de Kluijver et al. (2010) and Van den Meersche et al. (2011). A detailed article about the model is in preparation (Van Engeland et al., 2012). The model equations are also found in the supplementary material, there, phytoplankton is named phyto I and mixotrophs are named phyto II. The model code is incorporated in an R package, which is available upon request (R Core Team, 2012). Briefly, the concentrations of both ^{12}C and ^{13}C were modelled separately for the following carbon pools: phytoplankton, mixotrophs, labile DOC (LDOC), bacteria, zooplankton, detritus, and sedimented OM. The nitrogen pools explicitly described in the model were DIN and DON. Nitrogen fluxes relating to the other pools were calculated from carbon fluxes with a fixed Redfield stoichiometry. POC and PON were calculated in the model as the sum of phytoplankton and mixotrophs, bacteria, zooplankton and detritus. Light was used as forcing function for phytoplankton growth. The fractions of ^{13}C and ^{12}C in DIC were used as forcing functions for ^{13}C and ^{12}C incorporation by phytoplankton and mixotrophs, but no growth dependency on DIC (or CO$_2$) was built in the model. Bacterial biomass (based on PLFA; Fig. 1b) and zooplankton biomass (Niehoff et al., 2012) did not show large biomass changes during the experiment and were assumed to stay constant for model simplicity. Half-saturation constants for LDOC uptake by bacteria (ε_{DOC}) and zooplankton grazing on total phytoplankton (ε_g) were set to low values, assuming that they were used to low substrate values (oligotrophic conditions).
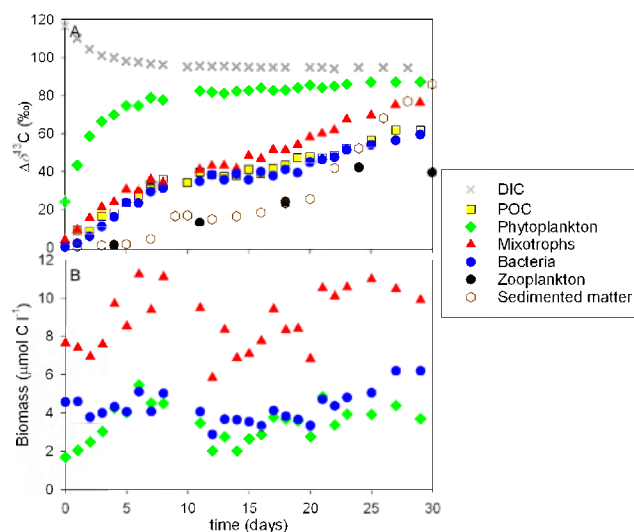

Fig. 1. The temporal change as averaged over all mesocosms ($n = 9$) of **(A)** isotope ratios ($\Delta\delta^{13}C$) of all measured carbon pools, and **(B)** of biomass (μmol C L^{-1}) of phytoplankton, mixotrophs, and bacteria.

The model was implemented in the open source software R (R Core Team, 2012), using the packages FME (Flexible Modelling Environment) and deSolve (Soetaert and Petzoldt, 2009; Soetaert et al., 2009). The output of the model was first manually fitted to the data to obtain good parameter fits. The data that were used to fit the model (observed variables) were phytoplankton, mixotrophs, bacteria, zooplankton, DIN, DON, POC, PON, and sediment POC and PON. The model was run separately before (phase 1) and after nutrient addition (phase 2). Good model fits were obtained for the first phase of the model (t_{0-12}). Unfortunately, no good fits could be obtained for phase 2 (t_{14-29}), primarily because of label saturation in phytoplankton, which precluded fitting the growth rate and subsequent exudation and mortality of phytoplankton during this phase. The fitted parameters were calibrated using the Markov Chain Monte Carlo (MCMC) technique (Gelman et al., 1996), as implemented in the FME package. A subset of parameters, potentially CO$_2$ sensitive, was calibrated with MCMC for each mesocosm. MCMC runs were accepted when they fell into the probability distribution centred around the current value (for details see Gelman et al., 1996). The model was run 5000 times for each mesocosm, resulting in $\sim$ 2000 accepted runs. The mean and standard deviation of the MCMCs were calculated for each parameter. The calibrated parameters were used to calculate fluxes (μmol C L^{-1} d^{-1}) between the carbon pools.

2.5 Statistics

Results are presented as average $\pm$ standard deviation (SD) over all mesocosms ($n = 9$). Simple Pearson correlation tests were used to test the effect of CO$_2$ on growth rates (Eq. 1),
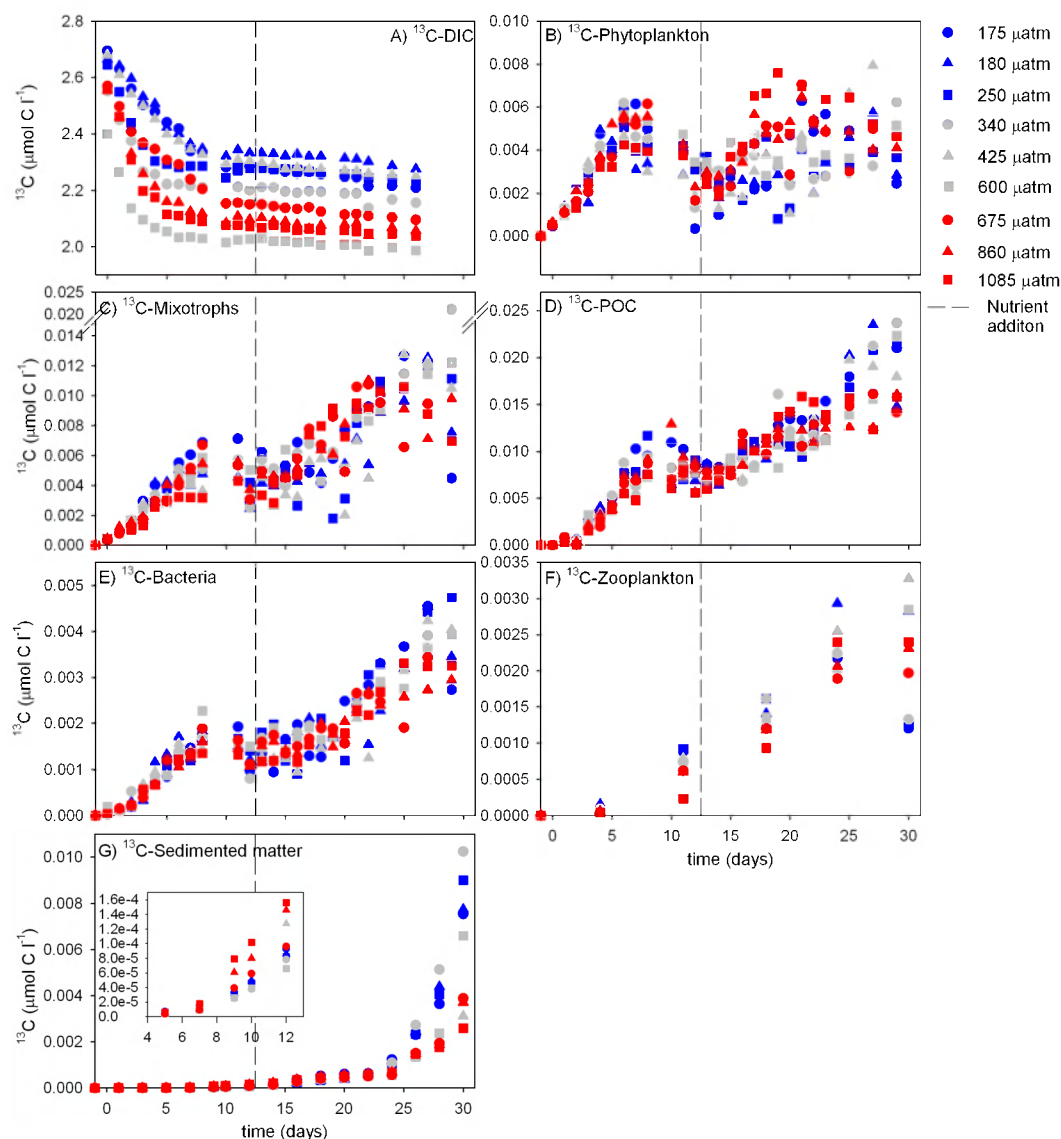
Fig. 2. Temporal development of ^{13}C in stocks and ^{13}C labelled biomass (μmol ^{13}C L^{-1}) of **(A)** DIC; **(B)** phytoplankton; **(C)** mixotrophs; **(D)** POC; **(E)** bacteria; **(F)** zooplankton (*Calanus* sp.); and **(G)** sedimented organic matter in each mesocosm. Red colours are used for high pCO$_2$ treatments, grey for medium, and blue for low pCO$_2$ treatments. The vertical line denotes the timing of nutrient addition. The inset of **(G)** zooms in on the first phase.

production rates (Eq. 3), linear increase in ^{13}C concentrations, and parameters and fluxes derived from the model. The results were tested and plotted against the average pCO$_2$ level in the corresponding phase. All statistical analyses were done in the software R.

3 Results

3.1 ^{13}C-DIC dynamics

Addition of 13C bicarbonate together with the first CO$_2$ addition on t_{-1} caused an increase in δ^{13}C of DIC of 117 ± 6 %

in all mesocosms (Fig. 1a). The decrease in $\Delta\delta^{13}$C-DIC in perturbed mesocosms during the first 4 days (t_{0-4}) can be largely explained by exchange with the dead volume, which was the space between the sediment traps and the bottom of the mesocosms and comprised ~ 10 % of total mesocosm volume (Schulz et al., 2012). Other processes that contributed to the initial label decrease were the subsequent (unlabelled) CO$_2$ additions, which diluted the ^{13}C-DIC pool and respiration of unlabelled organic material. The loss of ^{13}C-DIC due to air–sea exchange was low (< 0.15 %). From day 7 onwards, the $\Delta\delta^{13}$C of DIC remained quite stable (Fig. 1a). The labelled DIC concentrations were

Table 1. Growth (μ) and production (P) rates based on Eqs. (1) and (3), respectively, for each phase. Values are presented as average of all mesocosms $\pm$ standard deviation ($n = 9$).

	Growth rate (μ, d^{-1})			Production rate (P, μmol C L^{-1} d^{-1})		
	Phase 1 (t_{0-6})	Phase 1 (t_{0-12})	Phase 2 (t_{14-29})	Phase 1 (t_{0-6})	Phase 1 (t_{0-12})	Phase 2 (t_{14-29})
Phytoplankton	0.85 ± 0.06	0.19 ± 0.08	–	0.65 ± 0.08	0.19 ± 0.08	
Mixotrophs	0.48 ± 0.04	0.23 ± 0.02	0.22 ± 0.06	0.55 ± 0.06	0.30 ± 0.06	0.40 ± 0.13
Bac	0.68 ± 0.11	0.33 ± 0.02	0.13 ± 0.04	0.58 ± 0.05	0.47 ± 0.03	0.20 ± 0.15
POC					0.80 ± 0.13	0.75 ± 0.22

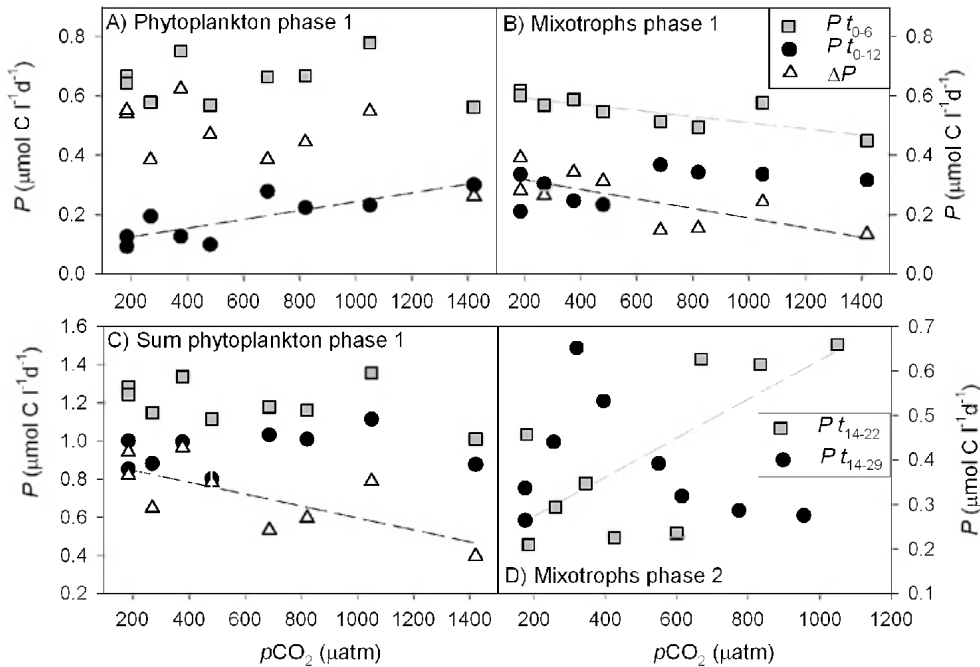**Fig. 3.** Production rates vs. average $p\mathrm{CO_2}$ levels of each phase based on data (Eq. 3) of **(A)** phytoplankton; **(B)** mixotrophs; and **(C)** sum phytoplankton and mixotrophs production rates (μmol C L^{-1} d^{-1}) in phase 1 for the build-up (t_{0-6}), the build-up and decline (t_{0-12}), and the production loss during decline (difference) denoted with ($\triangle$); **(D)** mixotroph production rates (μmol C L^{-1} d^{-1}) after nutrient addition for initial phase 2 (t_{14-22}) and total phase 2 (t_{14-29}).

2.6 ± 0.1 μmol ^{13}C L^{-1} at t_0 and decreased during the first 9 days to 2.2 ± 0.2 μmol ^{13}C L^{-1} at t_{10} and did not show large changes afterwards (Fig. 2a).

3.2 Phytoplankton and POC dynamics

After the enclosure of post-bloom water, a phytoplankton bloom developed even though inorganic nutrient concentrations were low (0.64 and 0.05 μmol L^{-1} DIN and phosphate, respectively). Phytoplankton rapidly incorporated ^{13}C; on t_7 the whole phytoplankton community had been turned-over, as indicated by the plateau (Fig. 1a), although phytoplankton never reached the $\Delta\delta^{13}$C of DIC. Mixotrophs showed clearly slower enrichment and never became saturated with ^{13}C (Fig. 1a). Phytoplankton initially had low biomass (1.2 ± 0.05 μmol C L^{-1}, $\sim 6\%$ of POC)

compared to mixotrophs (8.3 ± 1.2 μmol C L^{-1}, $\sim 40\%$ of POC) (Fig. 1b). A comparison with Chl a as a proxy for autotrophic biomass, and after subtraction of phytoplankton, indicated that $> 65\%$ of mixotroph biomass in phase 1 belonged to heterotrophs (Schulz et al., 2012, Czerny et al., 2012a). Both groups contributed to the bloom during phase 1 in biomass and reached a bloom peak at t_6 and declined afterwards (Fig. 1b). The development of ^{13}C labelled biomass showed that the bloom build-up and decline were more pronounced for phytoplankton compared to mixotrophs (Fig. 2b, c). This was also reflected in higher growth rates of phytoplankton (μ_{phyto}) compared to mixotrophs (μ_{mixo}) during bloom build-up (t_{0-6}). (Table 1). Bloom peak height, as well as growth rates of phytoplankton and mixotrophs were independent of $\mathrm{CO_2}$.

Table 2. Parameter descriptions and values of the food web model for phase 1 (t_{0-12}). Values are presented as average of all mesocosms $\pm$ standard deviation $(n = 9)$ derived from MCMC fitting procedures.

Parameter	Unit	Description	Value
		Parameters that were tested for different CO_2 levels	
μ_{Phy}	d^{-1}	growth rate of phytoplankton	0.87 ± 0.013
μ_{Mix}	d^{-1}	growth rate of mixotrophs	0.18 ± 0.010
ξ_{Phy}	d^{-1}	mortality rate of phytoplankton	0.29 ± 0.081
ξ_{Mix}	d^{-1}	mortality rate of mixotrophs	0.045 ± 0.025
μ_g	d^{-1}	grazing rate of zooplankton	0.022 ± 0.005
γ_{Phy}	d^{-1}	exudation rate of phytoplankton	0.31 ± 0.023
γ_{Mix}	d^{-1}	exudation rate of mixotrophs	0.24 ± 0.017
μ_{Bac}	d^{-1}	growth rate of bacteria	0.36 ± 0.029
r_{sink}	d^{-1}	sinking rate of detritus	0.0082 ± 0.0048
ρ	d^{-1}	mineralisation rate	0.020 ± 0.004
f_{DOM}	–	part of phyto mortality to DOM	0.056 ± 0.037
f_{Det}	–	part of phyto mortality to detritus	0.37 ± 0.05
		Parameters that were kept constant for different CO_2 levels	
ε_N	$\mu mol\,L^{-1}$	half saturation constant for DIN	0.5
ε_I	$W\,m^{-2}$	half saturation constant for light	120
ε_g	$\mu mol\,L^{-1}$	half saturation constant for phytoplankton + II	1
ε_{DOC}	$\mu mol\,L^{-1}$	half saturation constant for LDOC	0.001
f_{faeces}	–	part of zooplankton grazing to faeces	0.149
ξ_{Zoo}	–	part of zooplankton swimming into traps	0.654
NC	–	Stoichiometric ratio	16/106

Production of phytoplankton and mixotrophs during the build-up (t_{0-6}) averaged $1.20 \pm 0.11\,\mu mol\,C\,L^{-1}\,d^{-1}$. Production rates in overall phase 1, averaged over build-up and decline (t_{0-12}), were only $0.48 \pm 0.13\,\mu mol\,C\,L^{-1}\,d^{-1}$, due to the bloom decline after t_6 (Table 1, Fig. 3). Phytoplankton production during the build-up (t_{0-6}) was independent of CO_2, but the overall production (t_{0-12}) increased with increasing pCO_2 (Fig. 3a, $r = 0.81$, $p < 0.01$). Production rates of mixotrophs showed a different response to CO_2: the production rates during the build-up (t_{0-6}) were lower at higher pCO_2 (Fig. 3b, $r = -0.79$, $p < 0.05$) and overall production rates (t_{0-12}) were independent of CO_2. Despite contrasting responses to pCO_2, both phytoplankton groups had a loss in (particulate) production during the bloom collapse (t_{7-12}), which was CO_2 dependent (Fig. 3a, b). As a consequence, total production rates of phytoplankton (sum of phytoplankton and mixotrophs) were independent of pCO_2, but the loss in production during the bloom collapse (ΔP) was significantly higher at low pCO_2 than at high pCO_2 $(r = -0.70$, $p < 0.05$, Fig. 3c).

The production of phytoplankton and mixotrophs was reflected in the build-up of ^{13}C enriched POC with a peak on t_{8-11} and a subsequent decline (Fig. 2d). POC production averaged $0.80 \pm 0.13\,\mu mol\,C\,L^{-1}\,d^{-1}$ (Table 1). POC production was independent of CO_2 in phase 1, in agreement with the dynamics of the sum of phytoplankton (Fig. 3c).

After nutrient addition, phytoplankton and mixotrophs increased again in biomass, but there was more variation between mesocosms. Bloom peaks of phytoplankton were reached on t_{18-29}, depending on the mesocosm, but not on CO_2 (Fig. 2b). Bloom peaks of mixotrophs were reached on t_{22-29} and were also independent of CO_2 (Fig. 2c). Although ^{13}C biomass of mixotrophs kept increasing, total biomass, growth and production rates of mixotrophs after nutrient addition remained similar to phase 1 (Fig. 1b, Table 1). Production rates of mixotrophs were initially higher in the high CO_2 treatments $(t_{14-22}, r = 0.72$, $p < 0.05$, Fig. 3d). However, overall production rates in phase 2 (t_{14-29}) showed an optimum around current CO_2 levels (Fig. 3d). Because of label saturation (Fig. 1a), growth and production rates could not be determined for phytoplankton after nutrient addition. Also, POC production rates before and after nutrient addition were similar (Table 1, Fig. 4a). The average production rate of POC after nutrient addition (t_{14-29}) decreased with increasing CO_2 $(r = -0.87$, $p < 0.01$, Fig. 4a).

3.3 ^{13}C labelling of bacteria and zooplankto consumers

Heterotrophic bacteria followed the labelling pattern of POC (Fig. 1a). Initial bacterial biomass was $4.6 \pm 0.6\,\mu mol\,C\,L^{-1}$ $(\sim 19\,\%$ of POC) and stayed constant during phase 1

Table 3. Carbon fluxes (μmol C L^{-1} d^{-1}) in phase 1 (t_{0-12}) derived from the model between the major carbon pools, shown as arrows in Fig. 7. The values present the average $\pm$ standard deviation of all mesocosms ($n = 9$).

Processes	Flux (μmol C L^{-1} d^{-1})
Total primary production	1.78 ± 0.17
Phytoplankton production	1.17 ± 0.10
Production of mixotrophs	0.61 ± 0.09
Phytoplankton exudation	0.36 ± 0.05
Exudation by mixotrophs	0.19 ± 0.03
Bacterial production	0.60 ± 0.062
Zooplankton production	0.19 ± 0.04
Faeces production	0.028 ± 0.007
Phytoplankton mortality	0.60 ± 0.062
Mortality of mixotrophs	0.21 ± 0.11
Mortality to DOC	0.044 ± 0.029
Respired mortality	0.47 ± 0.093
Mortality to detritus	0.30 ± 0.074
Export of detritus	0.021 ± 0.093
Total export	0.13 ± 0.018

(Fig. 1b). Due to label incorporation, the ^{13}C-enriched bacteria biomass increased in the first phase and peaked on t_{6-8} (Fig. 2e). Bacterial production in phase 1 started with $0.58 \pm 0.05 \mu$mol C L^{-1} d^{-1} (t_{0-6}), but declined with the bloom collapse to 0.47μmol C L^{-1} d^{-1}, a production rate similar to primary production. Bacterial ^{13}C biomass increased again after nutrient addition until the end of the experiment. Both growth and production of bacteria were twice as high before rather than after nutrient addition (Table 1). Bacteria growth and production were independent of CO_2 levels.

Zooplankton (*Calanus* sp. and *Cirripedia*) incorporated ^{13}C in a similar way and the incorporation of tracer into copepods was used as representative for the mesozooplankton community. The ^{13}C incorporation into zooplankton was low (Fig. 1a). With a constant biomass of $\sim 5 \mu$mol C L^{-1} (Niehoff et al., 2012), the ^{13}C showed a negative correlation with CO_2 ($r = -0.92$, $p < 0.001$, Figs. 2f, 4b). From day 24 onwards, the variance in ^{13}C biomass increased and the CO_2 effect disappeared (Fig. 2f).

3.4 ^{13}C labelling of sedimented organic material

The label enrichment in sediment trap organic matter in the first 7 days was low, indicating that little freshly produced material was sinking into the traps (Fig. 1a). After day 7, the material became more enriched, probably because of the bloom collapse and after day 20, the $\Delta\delta^{13}$C of sediment trap POC increased rapidly (Fig. 1a). After day 25, the $\Delta\delta^{13}$C of sediment POC was higher than of water column POC, showing that there was preferential sinking of freshly produced material. The cumulative ^{13}C of sediment trap POC
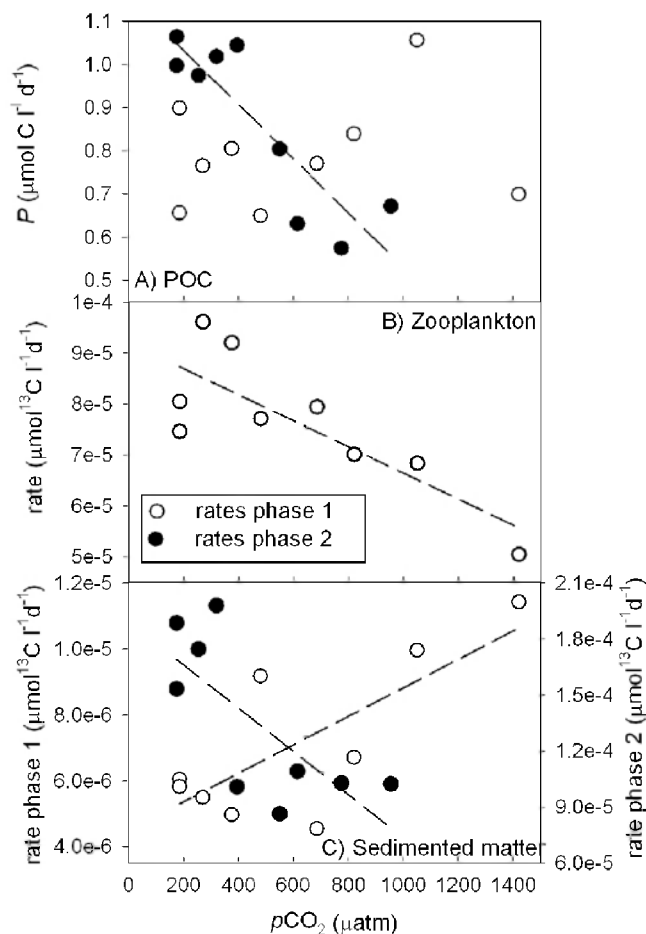

Fig. 4. (A) POC production (μmol C L^{-1} d^{-1}) before (phase 1) and after nutrient addition (phase 2); **(B)** ^{13}C increase in zooplankton (μmol ^{13}C L^{-1} d^{-1}) from t_{0-18}; **(C)** ^{13}C increase in cumulative sedimented organic matter (μmol ^{13}C L^{-1} d^{-1}) before (phase 1) and after nutrient addition (phase 2) as a function of average pCO$_2$ levels of the corresponding phase.

is shown in Fig. 2g. The settling of ^{13}C enriched POC in the traps was very low in the first phase and increased with increasing CO_2 ($r = 0.75$, $p < 0.05$, Fig. 4c). After nutrient addition, the sinking of ^{13}C-POC was much higher and the effect of CO_2 on sedimentation was reversed compared to phase 1 (Figs. 2g, 4c); sedimentation of freshly labeled (^{13}C enriched) POC decreased with increasing CO_2 ($r = -0.78$, $p < 0.05$, Fig. 4c). The ^{13}C increase in POC in the water column and sediment traps showed a non-linear response to CO_2 in phase 2, which indicates a step-wise rather than a gradual CO_2 effect (Fig. 4a, c). Mesocosms with CO_2 levels below 340 μatm had high POC production and sedimentation rates, while mesocosms with CO_2 above 400 μatm had low POC production and sedimentation rates after nutrient addition (Fig. 4a, c). The exception was at 395 μatm (average pCO$_2$ in phase 2) in the mesocosm where there was high production and low sedimentation (Fig. 2d, f). The fatty acid
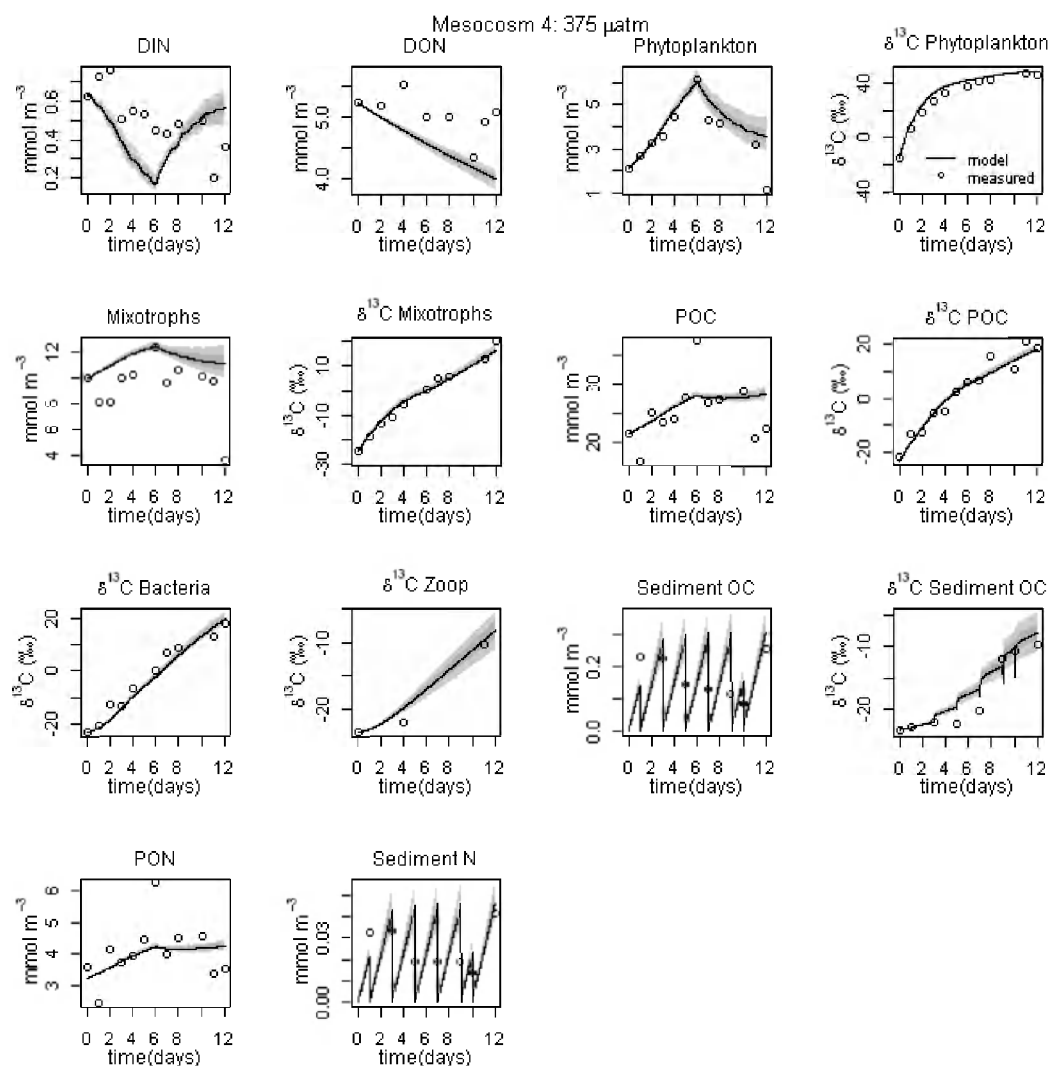
Fig. 5. MCMC plots showing the best fits of model output (solid line) with uncertainty (grey envelopes) fitted to the data (points) for one mesocosm (M4, 375 µatm). Fits of the other mesocosms are presented in the supplementary material.

composition of settling material in phase 3 revealed that all groups were present, but there were more mixotrophs' markers than phytoplankton markers in the sediment traps.

3.5 Model results: parameters and carbon fluxes

The construction of a model and subsequent fitting to the data provides the possibility to study the community as a whole, instead of studying carbon production in each carbon pool separately as done above. Fits for phase 1 of one mesocosm (M4, 375 µatm) are shown in Fig. 5 and the fits for the other mesocosms can be found in the supplementary material A. The set of parameters that were selected during the MCMC analysis was used to calculate average carbon fluxes over phase 1 (t_{0-12}).

The bloom of phytoplankton in phase 1 caused a decrease in DIN and DON concentrations (Fig. 5). Phytoplankton had

high growth rates (μ_{Phy}, Table 2) resulting in a large flux of DIC to phytoplankton (Table 3). Mixotrophs had lower growth rates (μ_{Mix}, Table 2) and lower primary production rates (Table 3). To reach the high biomass of phytoplankton, mortality was set to 0 during the first six days. Large parts from gross phytoplankton production were exuded as DOC; exudation averaged over all mesocosms $30.7 \pm 1.2\%$ of total primary production (for both phytoplankton and mixotrophs), which was subsequently used by bacteria. Bacteria had high growth rates (μ_{Bac}) and were the primary consumers, consuming $33.8 \pm 3.2\%$ of total primary production. Mesozooplankton had low grazing rates (μ_g) and consumed only $10.5 \pm 2.5\%$, on average, of total primary production in all mesocosms. The loss for bacteria was assumed to be respiration, while zooplankton loss was not only due to
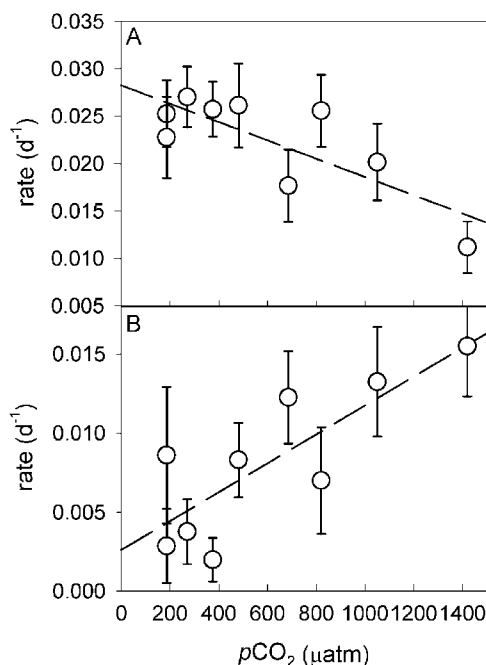
Fig. 6. Model parameters (d^{-1}) with uncertainties for **(A)** zooplankton grazing rates (μ_g) and **(B)** sinking rates (r_{sink}) vs. average pCO_2 levels in phase 1.

respiration (35 %), but primarily because of settling (65 %; ξ_{Zoo}).

Mortality after day 6 was higher for phytoplankton than for mixotrophs (Table 2). The mortality carbon flow was 51.3 ± 7.0 % of phytoplankton production and 36.2 ± 19.8 % of mixotroph production (Table 3). The largest fraction of plankton mortality was respiration, 37.0 ± 5.0 % went into detritus (f_{Det}) and 5.6 ± 3.7 % was channelled into DOC (f_{DOM}) (Table 2). The sinking rate (as fraction) of detritus (r_{sink}) was low $(0.0082 \pm 0.0048\,d^{-1}$ in all mesocoms) and also mineralisation (ρ) showed low rates (Table 2). Consequently, the export of detritus was low (Table 3). With the contribution of zooplankton to the sediment traps, the total export was 7.1 ± 1.4 % of total primary production averaged over all mesocosms.

Two of the twelve model parameters potentially sensitive to CO_2 showed to be indeed affected by CO_2 treatments. Grazing rates (μ_g) decreased with increasing CO_2 (Fig. 6a, $r = -0.79$, $p < 0.05$). Sinking rates (r_{sink}) showed a positive correlation with pCO_2 $(r = 0.81$, $p < 0.01$, Fig. 6b). The sinking was 5 times higher at high CO_2 $(0.016 \pm 0.0034\,d^{-1})$ compared to lower CO_2 $(0.0020 \pm 0.0014\,d^{-1})$. For validation of the parameters, the model was also tested with ξ_{Zoo} included as a CO_2 sensitive parameter. ξ_{Zoo} is the part of zooplankton carbon gain that ended in the sediment traps. ξ_{Zoo} was found to be CO_2 independent. The amount of zooplankters that ended in the traps were also independent of CO_2 levels (Niehoff et al., 2012).

The fluxes are graphically presented in Fig. 7, showing that the largest fluxes went from DIC to phytoplankton and subsequently bacteria. Because grazing rates and sinking rates were CO_2 sensitive (Fig. 5), the carbon flows from phytoplankton to zooplankton and detritus to sediment traps were also CO_2 sensitive as indicated by the dashed lines (Fig. 7).

4 Discussion

4.1 Plankton carbon flows under low nutrients

While most of the CO_2 enrichment mesocosm experiments involved inorganic nutrient addition and focussed on production and export food chains, this study investigated ocean acidification in a nutrient regenerating food chain, at least during phase 1 of the experiment. The low nutrient concentrations, low Chl a, and high heterotrophic biomass in Kongsfjorden waters were characteristic for a post-bloom situation (Rokkan-Iversen and Seuthe, 2011).

Although nutrient concentrations were low, a small phytoplankton bloom started right after enclosure, probably fuelled by efficient recycling of nutrients accompanied with remineralisation of DON, which decreased after the start of the experiment (Fig. 5, Schulz et al., 2012). Total net primary production rates in our experiment $(21\,mmol\,C\,m^{-2}\,d^{-1}$, average of all mesocosms integrated over the 12 m sampling depth) were similar to the median particulate primary production of $20\,mmol\,C\,m^{-2}\,d^{-1}$ in Arctic regions (synthesis by Kirchman et al., 2009a). However, net particulate primary production in this study was lower, $\sim 14\,mmol\,C\,m^{-2}\,d^{-1}$ (integrated over the 12 m sampling depth), suggesting nutrient limitation in our study. Primary production during the bloom was dominated by phytoplankton as indicated by their high growth and production rates (Tables 1, 2). Despite their low biomass, they were responsible for two thirds of the primary production in phase 1 (Tables 1, 3, Fig. 7).

According to flow cytometry, the productive phytoplankton consisted of nanophytoplankton during this time (Brussaard et al., 2013) and pigment analyses indicated that haptophytes were the main autotrophs (Schulz et al., 2012). The other third of primary production was contributed by the mixotrophs. Mixotrophs dominated in terms of biomass (Fig. 1b) and microscopy showed that they were mainly heterotrophic dinoflagellates and probably chrysophytes (Schulz et al., 2012). Regardless their high biomass, they had lower growth and production rates (Tables 1, 2, 3), as expected due to the mixotrophic character of the group.

The difference in model-based net primary production and data-based particulate primary production is the dissolved primary production: the release of organic matter. Two thirds of NPP was used for net particulate primary production $(1.2\,\mu mol\,C\,L^{-1}\,d^{-1}$, Table 1) and the other one third was exuded as dissolved primary production to fuel bacterial production. Bacteria were an important component of

the pelagic food web and a rapid consumer of primary production, as indicated by rapid transfer of label from phytoplankton to bacteria (Fig. 1a). Bacteria production amounted to a third of total phytoplankton production (34 %) (Table 3, Fig. 7). A remarkably similar average BP:PP ratio (34 %) was observed in Arctic transect studies by Kirchman et al. (2009b), although their absolute production rates were much lower.

The bacterial growth efficiency (BGE) during phase 1 was estimated to be ~ 15 % (Motegi et al., 2012), indicating that a large part of bacterial production was respired. High community respiration was also observed by Tanaka et al. (2012), who found respiration close to or sometimes exceeding primary production during phase 1. The net bacterial production under nutrient limitation was in the range measured with ^{3}H-thymidine (Table 2, Motegi et al., 2012). BP:PP ratios from our analyses were higher than those measured with ^{14}C during the same study (Engel et al., 2012). The discrepancy can be largely explained by their higher measured PP rates (Engel et al., 2012, and discussed therein). Bacterial growth rates in phase 1 (0.33–$0.36\,d^{-1}$) were rather similar to those measured with ^{14}C leucine: 0.24–$0.37\,d^{-1}$ (Piontek et al., 2012).

Despite the high growth rates, the biomass of bacteria did not increase (Fig. 1b), indicating a strong removal pressure (top–down control) on bacteria, e.g. by viruses or microzooplankton (heterotrophic dinoflagellates) grazing, which were both important during phase 1 (Brussaard et al., 2013; Schulz et al., 2012). Even an initial decline in bacterial numbers until $t\,5$ was determined with flow cytometry, although this was not seen in PLFA (Fig. 1b).

Although mesozooplankton were largely present (Niehoff et al., 2012), their grazing rates on primary production were very low, as indicated by maximum daily grazing rates of $0.022\,d^{-1}$ on phytoplankton biomass. In phase 1, only 11 % of primary production was consumed by mesozooplankton (Table 3, Fig. 7).

In summary, the high BP:PP, high microzooplankton abundance, and low mesozooplankton grazing indicate that the microbial food web was more important in this study than a herbivorous food web (Legendre and Razouldagan, 1995). Our results on plankton food web structure fit very well with the previously described post-bloom (May–July) situation in Kongsfjorden (Rokkan Iversen and Seuthe, 2011), with high BP:PP production and a prominent role for the microbial food web. However, they suggested a control of phytoplankton biomass by mesozooplankton grazing, because of low phytoplankton biomass, high primary production, and high zooplankton biomass, which is not supported by our findings.

Viral infection together with microzooplankton grazing likely caused the bloom to collapse after $t\,6$, since phytoplankton decline coincided with high microzooplankton grazing and increased virus abundance (Brussaard et al., 2013). Mortality affected phytoplankton much more than mixotrophs, consistent with virus–host specificity. Phytoplankton mortality rates of up to $0.3\,d^{-1}$, as observed for

phytoplankton, have been recorded during bloom declines as well as in oligotrophic systems (reviewed in Brussaard, 2004). When phytoplankton cells die, the cells lyse and a large portion is released as DOM, which can be subsequently used by bacteria (reviewed in Brussaard, 2004). In our study, phytoplankton mortality did not stimulate bacterial production per se, since bacterial production declined after day 6 as well (Table 2), but some DOC accumulation was observed (Czerny et al., 2012a; Engel et al., 2012). Possible explanations for the decline in bacterial production are concurrent viral infections or a shift from microzooplankton grazers from phytoplankton to bacteria.

Although it was difficult to constrain, we estimated that approximately one third of dying phytoplankton (phytoplankton mortality) ended up as detritus. Detritus formed only a small part of total POC produced (10 %) and was mainly formed of dead algae. The sedimentation losses of detritus were low ($0.008\,d^{-1}$) and in phase 1, sinking detritus comprised only 1 % of primary production (Table 3, Fig. 7). In phase 1, zooplankton contributed substantially to sedimented organic material (Niehoff et al., 2012). Together with zooplankton settling in the traps, the average export corresponded to $\sim$ about 7 % of primary production. In contrast, the calculated export in a previous mesocosm experiment with nutrient addition was ~ 24 times higher than the export rate in this experiment (Riebesell et al., 2007).

4.2 Plankton carbon flows after nutrient addition

The addition of nutrients did not increase total phytoplankton and bacterial biomass in the mesocosms (Fig. 1b). However, Chl a increased after nutrient addition (Schulz et al., 2012), indicating that the community shifted away from mixotrophy more towards autotrophy. Pigment and microscopy analyses indicated a shift in the autotrophic community towards dinoflagellates (Schulz et al., 2012), which are also part of the mixotrophs. Even though phytoplankton production increased the ^{13}C biomass (Fig. 2b, c), the total amount of phytoplankton carbon showed little increase (Fig. 1b). High grazing rates and viral lyses were factors that kept phytoplankton biomass low (Brussaard et al., 2013).

Interestingly, bacterial production and growth rates decreased after nutrient addition (Table 1), contrary to the generally observed positive relation between nutrient concentrations and growth efficiency (del Giorgo and Cole, 1998). Bacteria in phase 2 could have been limited by substrate (DOC) availability, since extra cellular release decreased after nutrient addition (Engel et al., 2012). In agreement with our findings, a similar decrease in bacterial growth from day 8 onwards was found with radioactive leucine incorporation during the experiment (Piontek et al., 2012).

The largest change in phase 2 compared to phase 1 was an increase in sedimentation. Large sedimentation of (freshly produced) organic matter occurred after day 24, when chain-forming diatoms started to grow in the mesocosms (Czerny
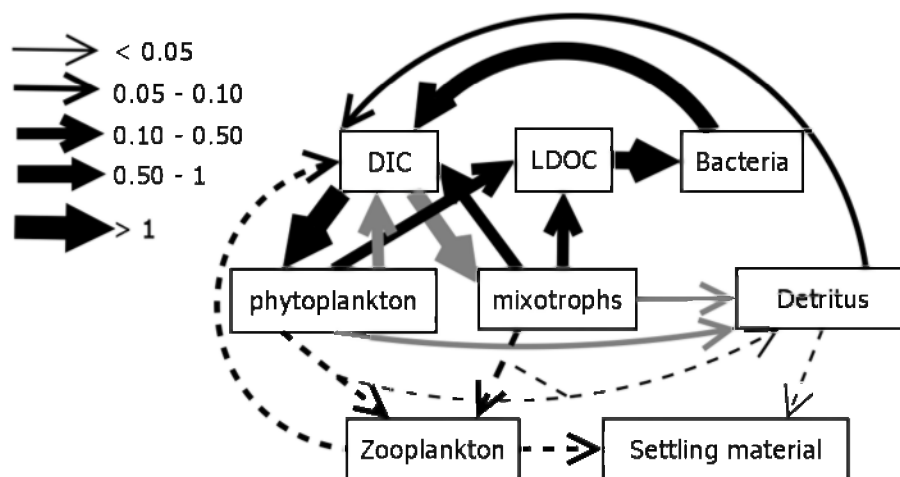
Fig. 7. Model-based carbon flow chart of phase 1 (before nutrient addition). The thicknesses of the arrows represent the size of the average carbon fluxes ($\mu mol\, C\, L^{-1}\, d^{-1}$) between the major carbon pools. The dashed arrows indicate fluxes that were CO_2 sensitive (based on model). The grey arrows indicate fluxes that may depend on pCO_2 based on data analyses (Fig. 3).

et al., 2012a). The diatoms probably formed aggregates that facilitated sinking of organic matter. The higher isotopic enrichment of sedimented organic matter compared to the water column (Fig. 1a) showed that the aggregates were formed of freshly produced organic matter and the dominance of diatoms was confirmed by the high presence of mixotroph markers in the sediment trap material.

4.3 Methodological considerations and assumptions

^{13}C labelling combined with modelling has been used successfully in previous mesocosm studies, allowing quantifying carbon flows and interactions in plankton food webs (Van den Meersche et al., 2004, 2011; de Kluijver et al., 2010). However, there are some assumptions and potential errors that need attention. A main advantage of using a ^{13}C tracer is that production can be measured in situ, in contrast to other methods like radioactive tracers that require side incubations with perturbed environmental (e.g. light) conditions. Using PLFA biomarkers, phytoplankton and bacteria group specific primary production can be estimated in addition to total POC production (Dijkman et al., 2009). A comparison of community production measurements performed during the experiment with different methods (DIC, oxygen, ^{13}C) is presented in Tanaka et al., 2012. There was a good correlation between ^{13}C-POC and DIC-based NCP, as we expected, since they were both measured in situ .

Although PLFAs can be used as taxonomic markers, the majority of PLFA markers do not allow distinction between heterotrophic and autotrophic (phyto)plankton, such as mixotrophic dinoflagellates, and therefore we had to consider them together as mixotrophs. To separate autotrophic and mixotrophic phytoplankton, additional methods are needed, such as fluorescence activated cell sorting combined with PLFA analysis (Pel et al., 2004). Because fatty acids

are often shared among taxonomic groups, we choose a conservative approach to consider only two phytoplankton groups based on their ^{13}C uptake patterns (phytoplankton and mixotrophs). However, temporal changes in total fatty acid composition were observed by Leu et al. (2012), indicating shifts in community composition within the two groups. An assumption, potentially introducing errors, was the application of a single conversion factor for PLFA:OC. Because we lacked (1) detailed species composition, (2) single-species biomarkers and (3) specific PLFA:OC ratios for each species, grouping phytoplankton and applying a single conversion factor seemed the most appropriate approach. Another assumption was that branched fatty acids are representative for the whole bacterial community, even though they primarily occur in gram-positive bacteria (Kaneda, 1991). Part of the (gram-negative) bacteria might have been overlooked, resulting in a potential underestimation of bacterial biomass and production, although the PLFA-based growth and production rates were in the range reported by Motegi et al. (2012) and Piontek et al. (2012).

The ^{13}C incorporation method is limited when phytoplankton is saturated with tracer, i.e. it has taken the signature of the source corrected for fractionation, in which case uptake of substrate will not cause further changes in ^{13}C. Saturation was observed in phytoplankton after the first six days precluding growth estimates after this period and precluding model application for phase 2. For future experiments an additional ^{13}C spike with nutrient addition is recommended. The other carbon pools did not get saturated with tracer (Fig. 1a) and bacteria never reached the isotope labelling of phytoplankton (Fig. 1a). Assuming that phytoplankton derived matter is the only carbon source for bacteria, this implies a senescent or dormant pool of bacteria that did not grow during the experiment.

Zooplankton never reached label enrichment of any carbon pool (Fig. 1a). Mesozooplankton has a slow turnover in response to dietary changes, contributing to low labelling patterns. A study on carbon turnover in Arctic crustaceans showed low turnover in stable isotopes with a half-life of 14 days (Kaufman et al., 2008). For simplicity, a uniform grazing rate on total phytoplankton was assumed in the model, but there was probably selective grazing on different phytoplankton groups. Due to the labelling differences between phytoplankton and mixotrophs, grazing rates would decrease if zooplankton primarily grazes on phytoplankton and increase if zooplankton primarily grazes on mixotrophs.

Another assumption was the application of a fixed Redfield stoichiometry in the model to fit the nitrogen fluxes (Table 2), although there was variability in this ratio (Schulz et al., 2012). Sensitivity of the fitted parameters to variable stoichiometry was tested and a variable stoichiometry showed little effect on parameter fitting (Van Engeland et al., personal communication). Potential changes in stoichiometry are a primary interests in ocean acidification research (e.g. Riebesell et al., 2007), but changes in stoichiometry seemed independent of CO_2 in this study (Schulz et al., 2012).

Production processes are relatively easy to determine with ^{13}C incorporation, but it is more challenging to quantify and allocate loss processes. The partitioning of carbon from phytoplankton mortality was difficult to constrain (Van Engeland et al., 2012). The partitioning in the particulate fraction was relatively easy to determine, because of direct POC measurements, but partitioning into dissolved material was more difficult, because of lack of accurate ^{13}C-DOC measurements. In our study, the amount of tracer added was insufficient to measure ^{13}C enrichment in DOC, due to the high background pool of DOC. For sufficient ^{13}C enrichment in DOC, the amount of added tracer should be > 10 times higher.

The data from the sediment trap samples have to be considered with care. The sediment traps were positioned only ~ 15 m deep, so the material in the sediment traps cannot be quantitatively considered to be exported compared to studies where traps were placed below the euphotic zone. The sediment traps were also within the daily migration zone of zooplankton and there were a large number of *Cirripedia* settling in the sediment traps. Zooplankton can contribute largely to settling material, especially in shallow traps, and contributions of 14–90 % of zooplankton to POC in traps were reported by Buesseler et al. (2007). In the model, an 82 % contribution of zooplankton to sediment trap material was necessary to achieve the low labelling of sediment material in phase 1. Preferential settling of old, unlabelled material in the traps could have contributed to the low labelling as well, but this was not considered in the model.

Although the above processes can cause potential errors in the estimated carbon fluxes, they do not explain the observed CO_2 effects, since they are expected to occur in all mesocosms.

4.4 CO_2 effects

In this study, we aimed to increase our understanding of CO_2 effects on primary production, community respiration, and export in Arctic communities by looking at individual uptake and loss rates and by quantifying the interactions between food web compartments with a food web model. Some of the CO_2 effects in phase 1 that were observed in individual fluxes (grey arrows in Fig. 7) were not shown in the integrated food web model, so we consider them with care.

Although it was not captured by the model, the data suggest that reduction in phytoplankton production due to phytoplankton mortality can be CO_2 sensitive. When the bloom collapsed (after $t6$), the loss in particulate primary production was significantly lower at higher CO_2 levels (Fig. 3c). A similar CO_2 effect on production losses in nanophytoplankton was seen, where production loss was twice as much at low CO_2 compared to high CO_2 (Brussaard et al., 2013). Reduced grazing by mesozooplankton at high CO_2 (Fig. 5b) can partly explain the reduced loss at high CO_2. However, grazing fluxes were too low (Table 3) to cover the differences in loss. Another explanation is the presence of CO_2 effects on the partitioning of phytoplankton mortality in phase 1. Both simple regression (Fig. 4c) and model output (Fig. 6b) showed that sedimentation of fresh organic matter increased with increasing CO_2 in phase 1. Since mortality rates were not sensitive to CO_2 and viral numbers were not CO_2 dependent (Brussaard et al., 2013), we speculate that there were CO_2 effects on the partitioning of dead phytoplankton in particulate and dissolved organic matter fractions. The organic material released at high CO_2 could be of a more sticky nature, serving as precursor of transparent exopolymer particles (TEP), or less degradable (Engel et al., 2002; Czerny et al., 2012a; Engel et al., 2012). When more dead phytoplankton ends in aggregates or particles, it could lead to enhanced sinking at high CO_2, as observed in phase 1.

Both simple regression (Fig. 4b) and model output (Fig. 6a), showed reduced zooplankton grazing in phase 1 with increasing CO_2. There was no CO_2 effect found on zooplankton numbers (Niehoff et al., 2012) and we can only speculate about the mechanisms. Reduced grazing could result from the reduced initial production of mixotrophs at higher CO_2 (Fig. 3b). Another possible explanation for reduced grazing could be CO_2 induced changes in food quality, i.e. the production of less essential fatty acids. Organic matter at high CO_2 contained less 22:6ω3 (Leu et al., 2012). 22:6ω3 is an essential fatty acid for zooplankton and can be growth limiting (Anderson and Pond, 2000). A hampering CO_2 effect on *Cirripedia* development to the next stage was observed (Niehoff et al., 2012), but whether this was related to lower grazing, needs to be further addressed.

In this study, no CO_2 effect on bacterial growth and production were observed. There was also no CO_2 effect on carbon exudation by phytoplankton as source for bacteria, although this process is considered potentially CO_2 sensitive.

It has been hypothesized that increasing CO_2 could stimulate carbon overconsumption and subsequent extracellular release, but most studies done so far showed no effects on DOC production in community-level CO_2 enrichment (e.g. Engel et al., 2004b). Previous mesocosm studies focussed on nutrient replete situations and it was suggested that CO_2 effects on extracellular release would be more pronounced under nutrient limitation (Thingstad et al., 2008; de Kluijver et al., 2010). The results here show that bacterial production on phytoplankton exudation is also not enhanced with CO_2 in a post bloom situation. However, a lack of bacterial response does not necessary mean that there was no stimulation of extracellular release by phytoplankton. Exudates are also important players in formation of TEP, marine snow and subsequent export (Engel et al., 2004a).

After nutrient addition, phytoplankton production rates (mixotrophs) were initially stimulated by higher CO_2 (t_{14-22}). The positive effect of CO_2 acted mainly on (autotrophic) dinoflagellates, shown by pigment analyses and microscopy (Schulz et al., 2012) and a relative fatty acid composition (Leu et al., 2012). Another group that benefitted from increased CO_2 were prasinophytes, which were part of phytoplankton (Schulz et al., 2012). The higher production of phytoplankton at high CO_2 in phase 1 (Fig. 3a) could have initialized this trend. Unfortunately, we could not measure production rates of phytoplankton after nutrient addition.

Mixotroph production showed an optimum around current CO_2 levels of 340 µatm over the whole phase after nutrient addition (t_{14-28}; Fig. 3c). The response of mixotrophs was likely an indirect effect of CO_2 due to competition with other phytoplankton groups. The proposed mechanism (based on pigments and flow cytometry) is that increasing CO_2 stimulated picoplankton directly after nutrient addition, leaving less dissolved inorganic nutrients for larger phytoplankton, like diatoms, in the final stage of the experiment (Schulz et al., 2012). The response to CO_2 after nutrient addition was also not gradual for POC production and sedimentation rates. POC production rates after nutrient addition showed a stepwise response to CO_2 with a transition point around current CO_2 levels (Fig. 4a). Production rates were lower at CO_2 levels above 400 µatm and because of the large export in phase 3, the CO_2 effect on POC production was directly reflected in settling material (Fig. 4c). Our findings suggest that CO_2 effects on some processes are stepwise rather than gradual, which can be of interest for future research.

5 Conclusions

This mesocosm study is the first to study ocean acidification effects on Arctic plankton communities in a system dominated by regenerated production. Before nutrient addition (phase 1), the pelagic food web was characterized by high BP:PP, high micro-zooplankton abundance, low mesozooplankton grazing and low export. Comparable production

rates, but increased export were observed after nutrient addition (phase 2). CO_2 effects were subtle and different for each phase. We observed a stimulating effect of CO_2 on export and a hampering effect on community (mesozooplankton) respiration in phase 1 and a hampering effect of CO_2 on production and export in phase 2. The observed CO_2 related effects potentially alter future organic carbon flows and export, with possible consequences for the efficiency of the biological pump.

References

Adolf, J. E., Place, A. R., Stoecker, D. K., and Harding, L. W.: Modulation of polyunsaturated fatty acids in mixotrophic Karlodinium veneficum (Dinophyceae) and its prey, Storeatula major (Cryptophyceae) 1, J. Phycol., 43, 1259–1270, doi:10.1111/j.1529-8817.2007.00419.x, 2007.

Algaier, M., Riebesell, U., Vogt, M., Thyrhaug, R., and Grossart, H.-P.: Coupling of heterotrophic bacteria to phytoplankton bloom development at different pCO$_2$ levels: a mesocosm study, Biogeosciences, 5, 1007–1022, doi:10.5194/bg-5-1007-2008, 2008.

Anderson, T. R. and Pond, D. W.: Stoichiometric theory extended to micronutrients: comparison of the roles of essential fatty acids, carbon, and nitrogen in the nutrition of marine copepods, Limnol. Oceanogr., 45, 1162–1167, 2000.

Bellerby, R. G. J., Schulz, K. G., Riebesell, U., Neill, C., Nondal, G., Heegaard, E., Johannessen, T., and Brown, K. R.: Marine ecosystem community carbon and nutrient uptake stoichiometry under varying ocean acidification during the PeECE III experiment, Biogeosciences, 5, 1517–1527, doi:10.5194/bg-5-1517-2008, 2008.

Bellerby, R. G. J., Silyakova, A., Nondal, G., Slagstad, D., Czerny, J., de Lange, T., and Ludwig, A.: Marine carbonate system evolution during the EPOCA Arctic pelagic ecosystem experiment in the context of simulated Arctic ocean acidification, Biogeosciences Discuss., 9, 15541–15565, doi:10.5194/bgd-9-15541-2012, 2012.

Bligh, E. G. and Dyer, W. J.: A rapid method of total lipid extraction and purification, Can. J. Biochem. Physiol., 37, 911–917, 1959.

Boschker, H. T. S. and Middelburg, J. J.: Stable isotopes and biomarkers in microbial ecology, FEMS Microbiol. Ecol., 40, 85–95, 2002.

Brussaard, C. P. D.: Viral Control of Phytoplankton Populations – a review: J. Euka. Microbiol., 51, 125–138, 2004.

Brussaard, C. P. D., Noordeloos, A. A. M., Witte, H., Collenteur, M. C. J., Schulz, K., Ludwig, A., and Riebesell, U.: Arctic microbial community dynamics influenced by elevated CO_2 levels, Biogeosciences, 10, 719–731, doi:10.5194/bg-10-719-2013, 2013.

Buesseler, K. O., Antia, A. N., Chen, M., Fowler, S. W., Gardner, W. D., Gustafsson, O., Harada, K., Michaels, A. F., van der Loeffó, M. R., Sarin, M., Steinberg, D. K., and Trull, T.: An assessment of the use of sediment traps for estimating upper ocean particle fluxes, J. Mar. Res., 65, 345–416, 2007.

Czerny, J., Schulz, K. G., Boxhammer, T., Bellerby, R. G. J., Büdenbender, J., Engel, A., Krug, S. A., Ludwig, A., Nachtigall, K., Nondal, G., Niehoff, B., Siljakova, A., and Riebesell, U.: Element budgets in an Arctic mesocosm CO_2 perturbation study, Biogeosciences Discuss., 9, 11885–11924, doi:10.5194/bgd-9-11885-2012, 2012a.

Czerny, J., Schulz, K. G., Ludwig, A., and Riebesell, U.: A simple method for air/sea gas exchange measurement in mesocosms and its application in carbon budgeting, Biogeosciences Discuss., 9, 11989–12017, doi:10.5194/bgd-9-11989-2012, 2012b.

de Kluijver, A., Soetaert, K., Schulz, K. G., Riebesell, U., Bellerby, R. G. J., and Middelburg, J. J.: Phytoplankton-bacteria coupling under elevated CO_2 levels: a stable isotope labelling study, Biogeosciences, 7, 3783–3797, doi:10.5194/bg-7-3783-2010, 2010.

del Giorgio, P. A., and Cole, J. J.: Bacterial growth efficiency in natural aquatic systems, Annu. Rev. Ecol. Syst., 29, 503–541, 1998.

DeLille, B., Harlay, J., Zondervan, I., Jacquet, S., Chou, L., Wollast, R., Bellerby, R. G. J., Frankignoulle, M., Borges, A. V., Riebesell, U., and Gattuso, J. P.: Response of primary production and calcification to changes of pCO_2 during experimental blooms of the coccolithophorid Emiliania huxleyi, Glob. Biogeochem. Cy., 19, GB2023, doi:10.1029/2004gb002318, 2005.

Dijkman, N. A. and Kromkamp, J. C.: Phospholipid-derived fatty acids as chemotaxonomic markers for phytoplankton: application for inferring phytoplankton composition, Mar. Ecol.-Prog. Ser., 324, 113–125, 2006.

Dijkman, N. A., Boschker, H. T. S., Middelburg, J. J., and Kromkamp, J. C.: Group-specific primary production based on stable-isotope labeling of phospholipid-derived fatty acids, Lim-

nol. Oceanogr. Methods, 7, 612–625, 2009.

Engel, A.: Direct relationship between CO_2 uptake and transparent exopolymer particles production in natural phytoplankton, J. Plankton Res., 24, 49–53, 2002.

Engel, A., Thoms, S., Riebesell, U., Rochelle-Newall, E., and Zondervan, I.: Polysaccharide aggregation as a potential sink of marine dissolved organic carbon, Nature, 428, 929–932, 2004a.

Engel, A., Delille, B., Jacquet, S., Riebesell, U., Rochelle-Newall, E., Terbruggen, A., and Zondervan, I.: Transparent exopolymer particles and dissolved organic carbon production by Emiliania huxleyi exposed to different CO_2 concentrations: a mesocosm experiment, Aquat. Microb. Ecol., 34, 93–104, 2004b.

Engel, A., Borchard, C., Piontek, J., Schulz, K., Riebesell, U., and Bellerby, R.: CO_2 increases ^{14}C-primary production in an Arctic plankton community, Biogeosciences Discuss., 9, 10285–10330, doi:10.5194/bgd-9-10285-2012, 2012.

Gelman, A.: Inference and monitoring convergence, Markov Chain Monte Carlo in practice, 131–143, 1996.

Grossart, H. P., Allgaier, M., Passow, U., and Riebesell, U.: Testing the effect of CO_2 concentration on the dynamics of marine heterotrophic bacterioplankton, Limnol. Oceanogr., 51, 1–11, 2006.

Kaneda, T.: Iso-fatty and anteiso-fatty acids in bacteria – biosynthesis, function, and taxonomic significance, Microbiol. Rev., 55, 288–302, 1991.

Kaufman, M., Gradinger, R., Bluhm, B., and O'Brien, D.: Using stable isotopes to assess carbon and nitrogen turnover in the Arctic sympagic amphipod Onisimus litoralis, Oecologia, 158, 11–22, doi:10.1007/s00442-008-1122-y, 2008.

Kirchman, D. L., Moran, X. A. G., and Ducklow, H.: Microbial growth in the polar oceans – role of temperature and potential impact of climate change, Natl. Rev. Micro., 7, 451–459, 2009a.

Kirchman, D. L., Hill, V., Cottrell, M. T., Gradinger, R., Malmstrom, R. R., and Parker, A.: Standing stocks, production, and respiration of phytoplankton and heterotrophic bacteria in the western Arctic Ocean, Deep-Sea Res. Pt. II, 56, 1237–1248, 2009b.

Leu, E., Daase, M., Schulz, K. G., Stuhr, A., and Riebesell, U.: Effect of ocean acidification on the fatty acid composition of a natural plankton community, Biogeosciences, 10, 1143–1153, doi:10.5194/bg-10-1143-2013, 2013.

Legendre, L. and Rassoulzadegan, F.: Plankton and nutrient dynamics in marine waters, Ophelia, 41, 153–172, 1995.

Middelburg, J. J., Barranguet, C., Boschker, H. T. S., Herman, P. M. J., Moens, T., and Heip, C. H. R.: The fate of intertidal microphytobenthos carbon: An in situ ^{13}C-labeling study, Limnology and Oceanography, 45, 1224–1234, 2000.

Motegi, C., Tanaka, T., Piontek, J., Brussaard, C. P. D., Gattuso, J. P., and Weinbauer, M. G.: Effect of CO_2 enrichment on bacterial production and respiration and on bacterial carbon metabolism in Arctic waters, Biogeosciences Discuss., 9, 15213–15235, doi:10.5194/bgd-9-15213-2012, 2012.

Niehoff, B., Knüppel, N., Daase, M., Czerny, J., and Boxhammer, T.: Mesozooplankton community development at elevated CO_2 concentrations: results from a mesocosm experiment in an Arctic fjord, Biogeosciences Discuss., 9, 11479–11515, doi:10.5194/bgd-9-11479-2012, 2012.

Pel, R., Floris, V., and Hoogveld, H.: Analysis of planktonic community structure and trophic interactions using refined isotopic signatures determined by combining fluorescence-activated cell

sorting and isotope-ratio mass spectrometry, Freshw. Biol., 49, 546–562, 2004.

Piontek, J., Borchard, C., Sperling, M., Schulz, K. G., Riebesell, U., and Engel, A.: Response of bacterioplankton activity in an Arctic fjord system to elevated pCO$_2$: results from a mesocosm perturbation study, Biogeosciences, 10, 297–314, doi:10.5194/bg-10-297-2013, 2013.

R Development Core Team: A language and environment for statistical computing, R Foundation for Statistical Computing, Vienna, Austria, ISBN 3-900051-07-0, www.R-project.org/, 2012.

Riebesell, U., Schulz, K. G., Bellerby, R. G. J., Botros, M., Fritsche, P., Meyerhofer, M., Neill, C., Nondal, G., Oschlies, A., Wohlers, J., and Zollner, E.: Enhanced biological carbon consumption in a high CO$_2$ ocean, Nature, 450, 545–549, 2007.

Riebesell, U., Kortzinger, A., and Oschlies, A.: Sensitivities of marine carbon fluxes to ocean change, Proc. Natl. Acad. Sci. USA, 106, 20602–20609, doi:10.1073/pnas.0813291106, 2009.

Riebesell, U., Czerny, J., von Bröckel, K., Boxhammer, T., Büdenbender, J., Deckelnick, M., Fischer, M., Hoffmann, D., Krug, S. A., Lentz, U., Ludwig, A., Muche, R., and Schulz, K. G.: Technical Note: A mobile sea-going mesocosm system – new opportunities for ocean change research, Biogeosciences Discuss., 9, 12985–13017, doi:10.5194/bgd-9-12985-2012, 2012.

Rivkin, R. B. and Legendre, L.: Biogenic carbon cycling in the upper ocean: Effects of microbial respiration, Science, 291, 2398–2400, 2001.

Rokkan Iversen, K. and Seuthe, L.: Seasonal microbial processes in a high-latitude fjord (Kongsfjorden, Svalbard): I. Heterotrophic bacteria, picoplankton and nanoflagellates, Polar Biol., 34, 731–749, 2010.

Schulz, K. G., Riebesell, U., Bellerby, R. G. J., Biswas, H., Meyerhöfer, M., Müller, M. N., Egge, J. K., Nejstgaard, J. C., Neill, C., Wohlers, J., and Zöllner, E.: Build-up and decline of organic matter during PeECE III, Biogeosciences, 5, 707–718, doi:10.5194/bg-5-707-2008, 2008.

Schulz, K. G., Bellerby, R. G. J., Brussaard, C. P. D., Büdenbender, J., Czerny, J., Engel, A., Fischer, M., Koch-Klavsen, S., Krug, S. A., Lischka, S., Ludwig, A., Meyerhöfer, M., Nondal, G., Silyakova, A., Stuhr, A., and Riebesell, U.: Temporal biomass dynamics of an Arctic plankton bloom in response to increasing levels of atmospheric carbon dioxide, Biogeosciences, 10, 161–180, doi:10.5194/bg-10-161-2013, 2013.

Soetaert, K. and Petzoldt, T.: FME: A Flexible Modelling Environment for inverse modelling, sensitivity, identifiability, monte carlo analysis, R package version, 1, 2009.

Soetaert, K., Petzoldt, T., and Setzer, R. W.: deSolve: General solvers for initial value problems of ordinary differential equations (ODE), partial differential equations (PDE) and differential algebraic equations (DAE), R package version, 1, 2009.

Steinacher, M., Joos, F., Frölicher, T. L., Plattner, G. K., and Doney, S. C.: Imminent ocean acidification in the Arctic projected with the NCAR global coupled carbon cycle-climate model, Biogeosciences, 6, 515–533, doi:10.5194/bg-6-515-2009, 2009.

Tanaka, T., Alliouane, S., Bellerby, R. G. J., Czerny, J., de Kluijver, A., Riebesell, U., Schulz, K. G., Silyakova, A., and Gattuso, J.-P.: Metabolic balance of a plankton community in a pelagic water of a northern high latitude fjord in response to increased pCO$_2$, Biogeosciences Discuss., 9, 11013–11039, doi:10.5194/bgd-9-11013-2012, 2012.

Thingstad, T., Bellerby, R., Bratbak, G., Børsheim, K., Egge, J., Heldal, M., Larsen, A., Neill, C., Nejstgaard, J., and Norland, S.: Counterintuitive carbon-to-nutrient coupling in an Arctic pelagic ecosystem, Nature, 455, 387–390, 2008.

Van den Meersche, K., Middelburg, J. J., Soetaert, K., van Rijswijk, P., Boschker, H. T. S., and Heip, C. H. R.: Carbon-nitrogen coupling and algal-bacterial interactions during an experimental bloom: Modeling a ^{13}C tracer experiment, Limnol. Oceanogr., 49, 862–878, 2004.

Van den Meersche, K., Soetaert, K., and Middelburg, J. J.: Plankton dynamics in an estuarine plume: a mesocosm ^{13}C and ^{15}N tracer study, Mar. Ecol.-Prog. Ser., 429, 29–43, doi:10.3354/meps09097, 2011.

Van Engeland, T., De Kluijver, A., Soetaert, K., Meysman, F., Middelburg, and J. J.: Model-based analysis of a mesocosm experiment: the added value of stable isotope tracer additions, in preparation, 2012.

Zelles, L.: Fatty acid patterns of phospholipids and lipopolysaccharides in the characterisation of microbial communities in soil: a review, Biol. Fertil. Soil., 29, 111–129, 1999.

Zhang, J., Quay, P. D., and Wilbur, D. O.: Carbon-isotope fractionation during gas-water exchange and dissolution of CO$_2$, Geochim. Cosmochim. Acta, 59, 107–114, 1995.